

ARTICLE OPEN



Real-time single particle characterization of oxidized organic aerosols in the East China Sea

Zhe Liu¹, Hui Chen^{1,2,✉}, Li Li², Guangzhao Xie¹, Huiling Ouyang³, Xu Tang³, Ruiting Ju¹, Bo Li¹, Renhe Zhang³ and Jianmin Chen^{1,3,✉}

Knowledge of the chemical characteristics and sources of organic aerosols (OA) over marine is needed for evaluating their effects on climate change and air quality. Here, a quadrupole aerosol chemical speciation monitor (Q-ACSM) and a single-particle aerosol mass spectrometry (SPAMS) were synchronously employed to investigate the chemical composition, mixing state, and oxidation degree of oxidized organic aerosols (OOA) in PM₁ over the East China Sea (ECS) from 3 to 27 June 2017. Both aerosol mass spectrometers demonstrated that a higher oxidation state of OOA in aerosol particles could be generated during marine air mass-dominated periods (MDP) than that generated during land air mass-dominated periods (LDP). Two OOA factors including semi-volatile oxidized organic aerosol (SV-OOA) and low-volatility oxidized organic aerosol (LV-OOA) were distinguished based on Q-ACSM. Fifty-seven percent of the total detected particles with obvious signals of organic markers were identified as oxidized organic carbon (OOC) particles via SPAMS and further divided into lower oxidized organic carbon (LOOC) particles and more oxidized organic carbon (MOOC) particles. All OOC-containing particles were clustered into seven particle subgroups. The EC and K subgroups dominated the LOOC and MOOC particles, respectively, during periods controlled by land air masses, indicating that notable OOC formation was influenced by continental sources. OOA with higher oxygen states were found to dominate near ports. This suggested that OOA chemical characteristics over the ECS are seriously affected by continental, ship, and port emissions, which should be synergistically considered in evaluating their effects on solar radiation transfer and cloud processes.

npj Climate and Atmospheric Science (2022)5:47; <https://doi.org/10.1038/s41612-022-00267-1>

INTRODUCTION

Oxidized organic aerosols (OOA) constitute an important component of ambient aerosols^{1–4} and can be produced through gas-to-particle partitioning of reaction products, oxidation of precursor volatile organic compounds (VOCs), and condensed-phase reactions in the atmosphere^{1,5}. OOA are characterized by substantially reduced saturation vapor pressures and therefore significantly contribute to new particle formation and growth of newly formed particles to cloud condensation nuclei (CCN) size⁶. OOA also adversely affect human health, as they can penetrate deep into the lungs to increase the risk of respiratory and cardiovascular diseases^{7,8}. In addition, certain chemical components are toxic, mutagenic, and carcinogenic, accruing serious health risks to humans not yet completely discovered⁹.

The formation processes and characteristics of OOA are affected by the type and quantity of the precursors, reactivity of the precursors and their oxidation products, and condensation trends of the oxidation and other reaction products¹⁰. In addition, meteorological parameters, such as the temperature (T) and relative humidity (RH), and NO_x level, in addition to the oxidant concentration [e.g., hydroxyl (OH), ozone (O₃), and nitrate (NO₃)], particle pH and aerosol liquid water content (ALWC), can all influence OOA formation. Due to their high temporal resolution, aerosol mass spectrometry (AMS) and aerosol chemical speciation monitor (ACSM) instruments have been widely employed in aerosol chemical composition measurements to investigate their chemical composition, sources, and secondary processes^{11–23}.

Generally, the OA types can be resolved via positive matrix factorization (PMF) according to the mass spectral signal, and OA can be classified into a primary organic aerosol (POA) [e.g., hydrocarbon-like OA (HOA), cooking OA (COA), and biomass burning OA (BBOA)] and OOA, which can be further resolved based on the oxidation degree [e.g., SV-OOA and LV-OOA]¹³. The contribution of OOA to OA exhibits wide spatial distributions, with a high fraction occurring at the background and rural sites, while a much lower fraction has been observed at urban and suburban sites due to the significant contribution of POA which can be generated mainly from anthropogenic emissions. For example, the contribution of OOA to OA reached 75% on the Qinghai–Tibet Plateau²⁴ and 41% in Beijing²⁵. Similar to the spatial distribution of the OOA fraction in OA, the contribution of LV-OOA generally shows an increasing trend from urban/suburban to background/remote sites, and LV-OOA dominated the OA composition with a contribution of 60.7% at Mt. Wuzhi²⁶. This is consistent with a previous study reporting gradually increasing LV-OOA contribution and O:C values from urban and suburban sites to background sites.

Knowledge of the mixing state of individual particles is crucial to understand their physicochemical properties better and provide information on their reaction processes. Single-particle mass spectrometry (SPMS), including aerosol time-of-flight mass spectrometry (ATOFMS) and single-particle aerosol mass spectrometry (SPAMS), can provide real-time mixing state and size information of individual particles²⁷, allowing insights into the

¹Shanghai Key Laboratory of Atmospheric Particle Pollution and Prevention (LAP3), National Observations and Research Station for Wetland Ecosystems of the Yangtze Estuary, Department of Environmental Science & Engineering, Fudan University, 200438 Shanghai, China. ²Key Laboratory of Organic Compound Pollution Control Engineering, School of Environmental and Chemical Engineering, Shanghai University, 200444 Shanghai, China. ³IRDR International Center of Excellence on Risk Interconnectivity and Governance on Weather/Climate Extremes Impact and Public Health, Institute of Atmospheric Sciences, Fudan University, 200438 Shanghai, China. ✉email: huichen@shu.edu.cn; jmchen@fudan.edu.cn

sources, atmospheric processes, and optical and cloud properties of atmospheric aerosols^{28–31}. Due to the application of a high-energy laser, single-particle aerosol mass spectrometry can measure not only water-soluble ions and organic matter but also non-refractory species such as metals. Currently, ATOFMS and SPAMS are widely adopted in source apportionment. For example, particles containing a mass spectrum involving strong K signals were identified as biomass burning particles^{32,33}. Healy et al.³⁴ measured the size and composition of freshly emitted ship exhaust particles at a port in Ireland, identifying a unique ship exhaust class containing internally mixed elemental and organic carbon, sodium, vanadium, nickel, calcium, iron, and sulfate. ATOFMS and SPAMS can identify both aged and freshly emitted particles. Many studies have demonstrated that aged particles are commonly internally mixed with secondary species of ammonium, nitrate, and sulfate through atmospheric processes^{35–37}.

Although SPMS can characterize almost all species to determine the chemical composition and mixing state of single particles at a high temporal resolution, it is difficult to obtain quantitative information due to its variable ionization and detection efficiency levels. As a result, it is crucial to integrate bulk and single-particle analysis results, which can provide more complete information on atmospheric aerosol particles. Middlebrook et al.³⁸ first operated AMS and ATOFMS instruments jointly, and subsequently, an increasing number of studies have employed these two instruments together^{39,40}. Drewnick et al.⁴¹ deployed AMS and ATOFMS instruments to characterize aerosols generated from lawn mowing and identified two aerosol sources, thus demonstrating that the combination of these two instruments could provide more comprehensive information to identify aerosol sources. Cubison et al.⁴² measured the size-resolved mass and size-resolved number concentration of aerosols to investigate the mixing state better. They verified that the aerosol mixing state is important in determining the activation properties of particles around the critical activation diameter to obtain atmospherically realistic supersaturating values. Salcedo et al.³⁹ compared the particle lead concentrations observed with AMS and ATOFMS instruments, indicating good agreement between these two instruments. AMS and laser desorption/ionization single-particle aerosol mass spectrometry (LISPA-MS) instruments were co-developed to characterize organic aerosols in Tokyo⁴⁰. The RCOO signal in LISPA-MS and the m/z 44 signal obtained with an AMS instrument exhibited a significant linear correlation, suggesting that the RCOO signal in LISPA-MS could be a measure of the relative abundance of OA. Approximately 95% of the organic containing particles identified via LISPA-MS contained nitrate, which explained the correlation between m/z 44 and nitrate observed with AMS instrument, facilitating the deeper investigation of the mixing state of OA and nitrate. All these studies suggest that the mixing state, oxidation condition, formation mechanisms, and sources of OA could be better revealed with the combined adoption of the two-particle mass spectrometers.

Covering over two-thirds of the Earth's surface, marine environments significantly impact the Earth's climate and notably contribute to global aerosols^{43–45}. The marine atmosphere is affected by anthropogenic sources, including industrial processes, fuel, and biomass burning through long-range transportation, ports, and shipping exhaust emissions, as well as biogenic emissions^{46–49}. A notable impact of biomass burning on the marine aerosol composition was observed during a campaign from the Cape Verdean island of São Vicente to Gabon, revealing elevated SOA concentrations⁵⁰. Recently, research has increasingly focused on the emissions of atmospheric pollutants originating from shipping, with the contributions to ambient $PM_{2.5}$ as $51.9–62.6 \mu\text{g}/\text{m}^3$ in China^{51,52} and $0.26–2.3 \mu\text{g}/\text{m}^3$ in Europe^{53–59}. The oxidation products of gas-phase species emitted from the ocean, including dimethyl sulfide (DMS) and other biogenic volatile organic compounds (VOCs), could be further converted

into OOA, which comprises an important marine aerosol source⁶⁰. Moreover, the chemical composition and properties of OOA in marine environments are influenced by meteorological factors such as air humidity, wind speed, and direction. However, the OOA characteristics on a single-particle basis and the influencing factors of the OOA oxidation degree remain unclear.

In this study, we carried out a cruise campaign in the offshore area of the ECS from 3 to 27 June 2017, presenting real-time measurements of marine ambient aerosol using Q-ACSM and SPAMS. The bulk OOA mass concentration and composition were quantitatively measured with the ACSM instrument, and the single-particle chemical composition was further investigated via SPAMS. The aims of this work are to (1) investigate the single-particle characteristics of OOA in the ECS (2) analysis the oxidation degree of OOA during different air mass-dominated periods, and (3) reveal the main factor influencing the OOA oxidation degree in the ECS. Combinatorial consideration of the obtained data on a bulk basis and a particle-by-particle basis could provide deeper insights into the OOA chemical characteristics, highlighting the anthropogenic activities influence on occurrence, sources, and formation of OOA in the ECS.

RESULTS

Overview of the bulk and individual measurements

Supplementary Figure 1 depicts 24 h backward trajectories of the air masses arriving at the sampling site. The entire study was separated into four stages by the air mass type. Stage 1 (S1) and stage 3 (S3) were marine air mass-dominated periods (MDP), while stage 2 (S2) and stage 4 (S4) were land air mass-dominated periods (LDP). Figure 1a shows the time series of the mass concentrations of NR- PM_{10} species including organics (Org), sulfate (SO_4), nitrate (NO_3), ammonium (NH_4), and chloride (Cl) and OA chemical components, and Supplementary Fig. 3 shows time series of the meteorological parameters and gaseous species. The concentration of the total NR- PM_{10} mass during the LDP was ~3 times higher than that during the MDP. SO_4 yielded a much greater contribution than that yielded by NO_3 during the MDP while attaining a similar concentration to that of NO_3 during the LDP, likely due to the high SO_2 emissions near ports as well as the contribution of marine emissions^{61–63}. With a range from $1.5–5.0 \mu\text{g}/\text{m}^3$, the contribution of OA varied within the narrow range of 27–36% during the campaign. The observed OA mass loadings were similar to other observations at the background site, while the fraction of OA was lower than that reported in previous studies, suggesting that the observation site was deeply affected by anthropogenic activities^{24,64}. Accounting for 53 and 51% of all OA during S1 and S3, respectively, LV-OOA contributed substantially to OA during the MDP but much less during the LDP. In contrast, the concentration of SV-OOA was higher during the LDP than that during the MDP (54–59% versus 19–32%). The LV-OOA/SV-OOA ratio was significantly elevated from the LDP (0.74 on average) to the MDP (2.16 on average), which suggests that the OOA oxidation degree was higher during the MDP.

Overall, a total of 546,874 particles with both positive and negative mass spectra were collected during the campaign, and 57% of these particles (by number) were identified as OOC particles. Among these particles, 50% of the OOC particles with a higher intensity of OOC markers were identified as MOOC particles, and the remaining particles were identified as LOOC particles⁶⁵. The number of total collected particles and OOC particles was compared to mass concentrations obtained with the ACSM instrument, as shown in Supplementary Fig. 7, and the MOOC/LOOC ratio was compared to the LV-OOA/SV-OOA ratio, as shown in Fig. 1c. Although the time series of the total particle counts and OOC particle counts did not indicate a completely consistent trend with that of the NR- PM_{10} and OOA mass

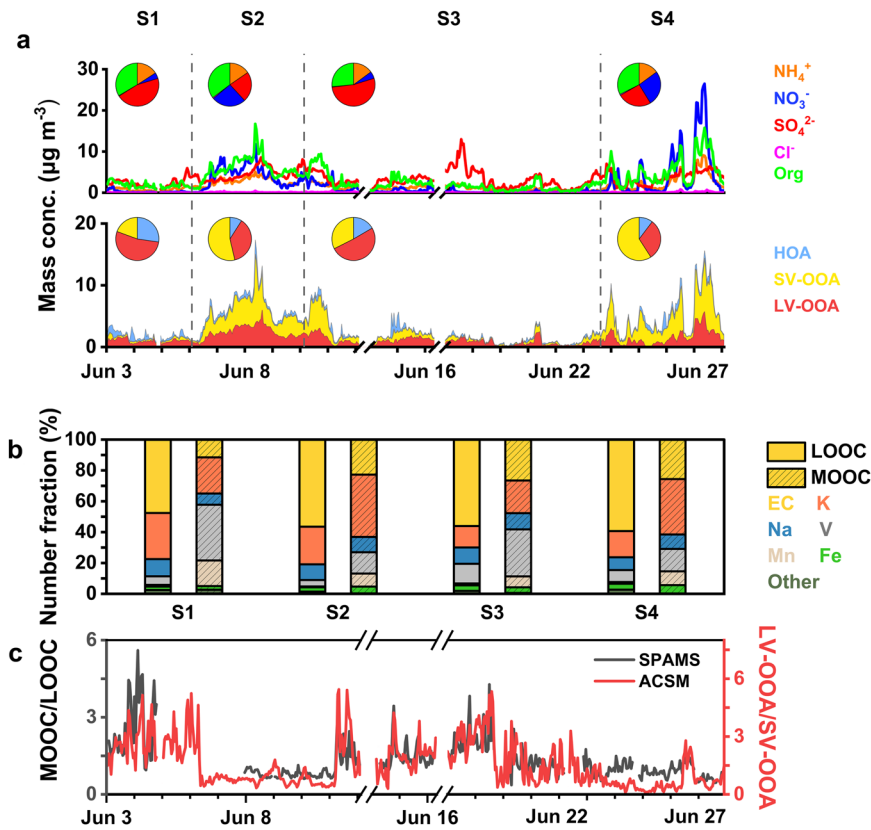


Fig. 1 Bulk and individual measurement results. **a** Time series of the NR-PM₁ and organic species concentrations at the four stages; **b** number fraction of the particle subgroups (EC, K, Na, V, Mn, Fe, and other subgroups) in the LOOC and MOOC particles at the four stages; **c** time series of the LV-OOA/SV-OOA values obtained with the ACSM instrument and MOOC/LOOC values obtained via SPAMS.

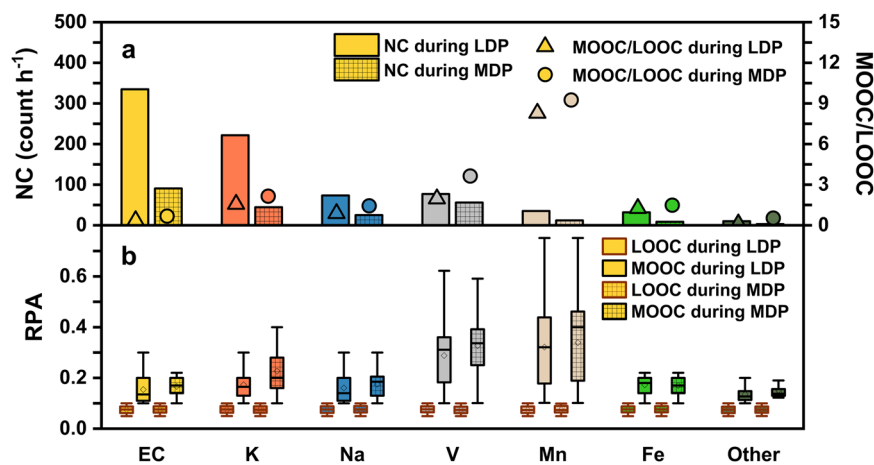


Fig. 2 Single-particle characterization of OOA. **a** Particle number concentration (NC) and MOOC/LOOC ratio during the LDP and MDP; **b** relative particle area (RPA) of the OOC markers in the LOOC and MOOC particles in every subgroup during the LDP and MDP. The diamonds indicate the mean values. The line inside the box indicates the median. The box and error bars indicate the 10, 25, 50, 75, and 90th percentiles.

concentrations because SPAMS cannot provide quantitative data, the time series of the MOOC/LOOC ratio was broadly similar to that of the LV-OOA/SV-OOA ratio, demonstrating that size-resolved chemical composition analysis via SPAMS can be combined with quantitative bulk concentration determination with ACSM instruments to study OOA.

To identify the characteristics and sources of individual OOC particles, we separated both MOOC and LOOC particles into 7 subgroups, including EC, K, Na, V, Fe, Mn, and other subgroups. Supplementary Figure 8 shows the time series and size

distributions of all subgroups. As shown in Fig. 2, the EC subgroup was the most abundant particle among the LOOC particles during the MDP, accounting for 48 and 56% of all particles during S1 and S3, respectively. EC particles were likely derived from incomplete combustion of carbon-containing compounds, such as vehicle emissions and fuel combustion⁶⁶. A large fraction of the V subgroup in the MOOC particles was observed during the MDP. V is a notable marker of ship emissions^{52,67}. The abundant V particles were associated with fresh aerosols emitted at ports and by ships and further underwent aging reactions, indicating the

significant influences of port and ship emissions on the OOA composition. Similar to the MDP, the EC subgroup yielded the largest contribution to the LOOC particles during the LDP. Accounting for 40 and 36% of all particles during S2 and S4, the K subgroup was the most abundant particle among the MOOC particles during the LDP, and the abundance was significantly higher than that during the MDP. K is often employed as notable biomass burning marker^{36,68} and the K subgroup became highly oxidized during long-range transportation from land to marine areas. The abundant K subgroup in the MOOC particles during the LDP suggested the important effects of land sources on OOA formation in the offshore area of the ECS. Even though mainly affected by marine air masses during S1, the K subgroup accounted for a high fraction of the LOOC particles since the ship sailed along with Shanghai and was influenced by anthropogenic activities on land.

Effects of the particle composition on the OOA oxidation degree

Supplementary Figure 5 shows the spatial distribution of OA along the cruise. The observed OA concentration at the different sites exhibited substantial spatial variance, with higher values near Shanghai and Ningbo and lower values near Zhoushan Island, which highlighted the effects of land sources on the OOA concentration. High OA concentrations were observed on 27 June (from QD to SS) due to the influence of land sources, even at relatively large distances away from land, which suggested that the air mass type dominated the OOA concentration in the offshore area of the ECS. We noted that higher LV-OOA/SV-OOA ratios were observed near ports, which indicates that the elevated oxidation degree of OOA was affected by ports. A similar result was also found in a previous study, in which it was observed that aged ship emissions prevailed over primary emissions in the port environment⁴⁸.

As discussed in section "Overview of the bulk and individual measurements", the air mass type influenced the OOC composition. We further compared the average particle number concentration between the two air mass-dominated periods. Even though higher particle number concentrations of all subgroups were observed during the LDP due to the significantly higher total particle counts, the EC and K subgroups revealed the most obvious increase, while the V subgroup exhibited a slight increase, indicating that land sources through transportation generated abundant EC and K particles. To explore the influence of the OOC composition on the OOA oxidation degree, we examined the MOOC/LOOC ratio in each particle subgroup during the LDP and MDP, as shown in Fig. 2a. Higher MOOC/LOOC ratios were observed in the Mn and V subgroups during both the LDP and MDP, indicating the high oxidation degree of Mn and V particles, respectively. Mn was found to catalyze the formation of sulfate during haze events in a recent study⁶⁹, which may also promote the formation of OOA. Enhanced oxalate production stemming from the oxidation of organic precursors was observed in V particles by Gong et al.⁷⁰, suggesting that the presence of V may substantially impact OOA production. The Mn subgroup yielded small and similar contributions during the LDP and MDP and was not the main factor causing the high MOOC/LOOC ratio during the MDP. V is largely introduced into the atmosphere via ship emissions, and V particles play an important role in offshore areas due to busy transportation activities. The high MOOC/LOOC ratio during the MDP was associated with the increased V particle contribution during these periods. The EC and K subgroups exhibited a lower MOOC/LOOC ratio than that in the V particles during both the LDP and MDP, especially the EC subgroup, which exhibited the lowest MOOC/LOOC value throughout the whole campaign. Air masses transported land pollutants during the LDP,

which considerably increased the fraction of EC and K particles, leading to a lower MOOC/LOOC ratio during the LDP.

To further examine the oxidation degree of every particle subgroup, the relative particle area (RPA) of OOC markers was compared between the different subgroups. The RPA of the OOC markers in the LOOC particles indicated no significant variance between the different subgroups due to the employed classification rules. Among the MOOC particles, the RPA of the OOC markers was higher for the Mn and V subgroups during both periods, followed by the Fe, K, Na, EC subgroups during the LDP and the K, Na, Fe, EC subgroups during the MDP. The higher RPA of the OOC markers in the Mn and V subgroups suggests that the organic material in these particles is susceptible to deeper oxidation processes.

Different OOA characteristics and formation influencing factors during the LDP and MDP

We noted that the MOOC/LOOC ratios were higher during the MDP than those during the LDP in every subgroup. As shown in Fig. 2, the MOOC/LOOC ratios in the V and EC subgroups during the MDP were approximately two times higher than those during the LDP. Except for the V and EC subgroups, all other subgroups showed a slightly increasing trend during the MDP over the LDP. To further explore the OOA oxidation degree, the van Krevelen diagram (V-K diagram) was applied to depict the H:C and O:C ratios⁷¹. As shown in the V-K diagrams in Fig. 3a and d, the O:C ratio varied between 0.4 and 0.9 during the LDP, which was lower than that during the MDP, with the O:C ratio ranging from 0.5 to 1.1. Previous studies reported a higher O:C ratio (ranging from 0.5 to 1.4) at background sites and a lower O:C ratio in urban areas (ranging from 0.3 to 0.6)^{72–74}, suggesting that organic aerosols could be more notably oxidized with fewer anthropogenic sources. The O:C ratio throughout the whole campaign was higher than that in observations in urban areas but slightly lower than that at background sites. The lower O:C ratio during the LDP was consistent with the increased effects of anthropogenic sources during these periods. The formation mechanism of OOA can be estimated according to the slope of the V-K diagram^{71,75}. The formation of alcohol and peroxide emerged as the dominant process for OOA during this campaign since the slopes in both V-K diagrams were close to -0.2 .

Figure 3b and e shows the average diurnal cycles of the OA species mass concentration during the LDP and MDP, respectively. OA exhibited distinct diurnal patterns during these two periods. During the LDP, SV-OOA exhibited a pronounced diurnal cycle with a distinct peak between 10:00 and 11:00, while LV-OOA exhibited a flat diurnal cycle. Comparatively, SV-OOA demonstrated a stable distribution, and LV-OOA revealed a gradual increase starting from 8:00 until 14:00 and then a decrease until 19:00 during the MDP. Photochemical and aqueous-phase processes exerted combined effects on OOA formation⁷⁶. Their influence on the OOA concentration and composition during the LDP and MDP are illustrated in Fig. 3c and f, respectively. The highest OOA mass concentration values occurred in the top right corner, indicating that both photochemical and aqueous-phase processes played an important role in the formation of OOA. However, the LV-OOA/SV-OOA ratio revealed a negligible relationship with the ALWC and O₃, which indicated that there are more factors influencing the OOA oxidation degree. During the MDP, the OOA concentration and the LV-OOA/SV-OOA ratio exhibited similar distributions, attaining high values at high O₃ concentrations. This indicated that photochemical processes dominated the formation of LV-OOA which is consistent with the peak value of the LV-OOA concentration at noon. To evaluate the contribution of photochemical and aqueous-phase processes to every subgroup during these two periods, the changes in the MOOC/LOOC value with the O₃ and ALWC concentrations during the LDP and

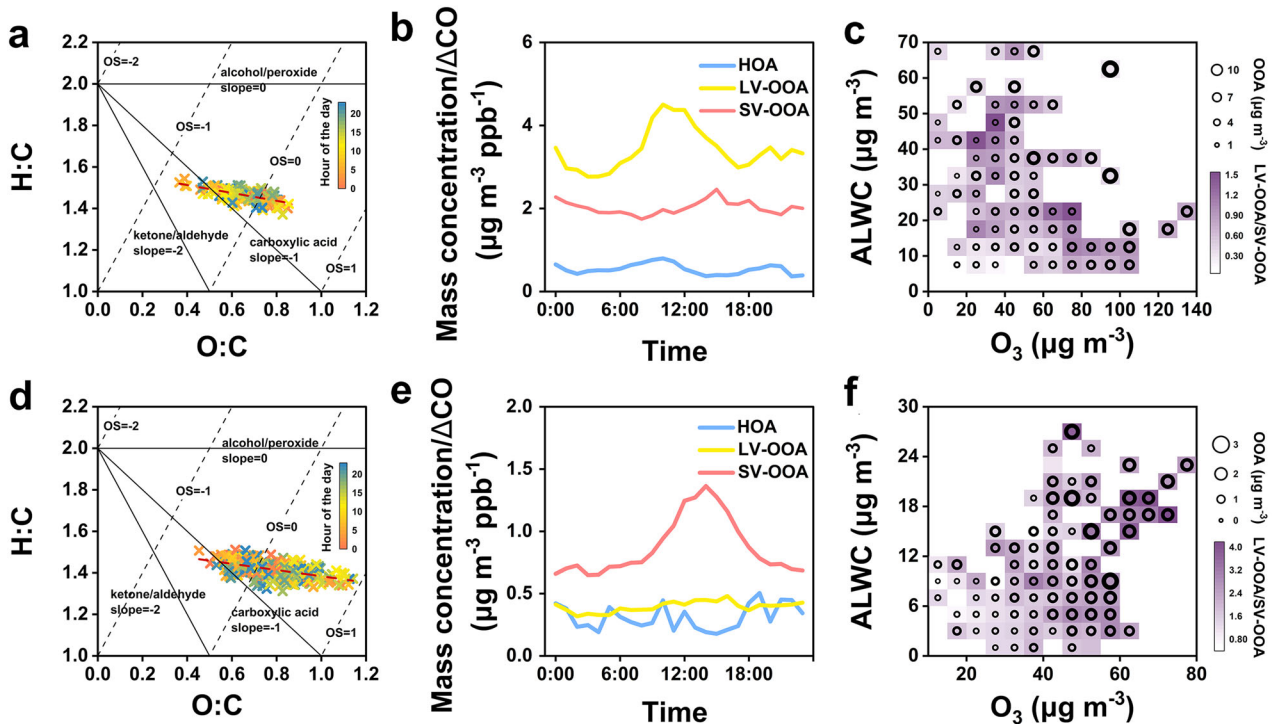


Fig. 3 Influence factors of OOA oxidation state. Van Krevelen diagram of the OOA during **a** the LDP and **d** MDP; diurnal patterns of the three types of OA (HOA, SV-OOA, and LV-OOA) during **b** the LDP and **e** MDP; ALWC and O_3 dependence of the OOA concentration and LV-OOA/SV-OOA ratio during **c** the LDP and **f** MDP, respectively.

MDP were investigated, as shown in Supplementary Fig. 9. Generally, the V and Mn subgroups exhibited increasing trends with increasing O_3 concentration during both periods, suggesting that photochemical processes played a more important role in OOA formation for the V and Mn subgroups. During the MDP, the MOOC/LOOC ratio in the EC and K subgroups increased dramatically with increasing O_3 concentration, while they exhibited a decreasing trend during the LDP, likely due to other influencing factors, such as campaign cruises.

Oxidation degree and evolution patterns of OOA and their subgroups

To further investigate the reason for the higher OOA oxidation degree during the MDP, we evaluated the contributions of the particle subgroup components and the oxidation degree of every subgroup during these two periods. Since the K, EC, and V subgroups accounted for the major fraction throughout the whole campaign, ternary plots (Fig. 4a and c) were generated to visualize the relationship between the LV-OOA/SV-OOA ratio and the fraction of these three subgroups.

Most particles during the LDP fell on the left side of the plot, illustrating that the K and EC subgroups continuously constituted the dominant fraction during the LDP. The particles during the MDP were scattered across the ternary plot, and the LV-OOA/SV-OOA ratio indicated an increasing trend near the corner at the right, which verifies that a large fraction of V particles during the MDP plays a significant role in the enhanced OOA oxidation degree. Figure 4b and d further shows the effects of the oxidation degree of the three subgroups on the LV-OOA/SV-OOA ratio. During the LDP, an increased proportion of MOOC particles in the K and EC subgroups was accompanied by a higher LV-OOA/SV-OOA ratio. Similar trends were also observed during the MDP. Higher LV-OOA/SV-OOA ratios were found over time higher LV-OOA/SV-OOA ratios. Additionally, we noted that certain points were scattered at the top of the ternary plot only during the MDP,

indicating a higher contribution of MOOC particles during the MDP. The points scattered at the top of the ternary plot indicated a higher LV-OOA/SV-OOA ratio, which suggests that a higher fraction of MOOC particles is a significant factor in the higher oxidation degree during the MDP.

Figure 5a shows the variance rate of SV-OOA and LV-OOA detected with the ACSM instrument as well as of the LOOC and MOOC particles detected via SPAMS. Broadly similar trends in the variance rates between the SV-OOA and LOOC particles and between the LV-OOA and MOOC particles were observed. In total, the variance rates of the SV-OOA and LV-OOA during the LDP were significantly higher than those during the MDP, which could further support the important contribution of land sources to the marine air environment. Three cases were selected further to illustrate the OOA evolution pattern at the different stages.

Figure 5b and c shows the variance process of two OOA and the variance ratios of seven subgroups in the three cases. The results reveal that different processes could be attributed to different components. With decreasing rates of $0.44 \mu\text{g m}^{-3} \text{h}^{-1}$ and $0.22 \mu\text{g m}^{-3} \text{h}^{-1}$, sharp declines in SV-OOA and LV-OOA were observed in Case 1, which were attributed to the dilution effect of clean marine air masses and less influenced by land pollutant sources. The EC subgroup, with a variance ratio of 94, contributed the most to the decrease in SV-OOA, followed by the K subgroup. We noted that V subgroup attained a negative variance ratio value, which was consistent with the increasing ship emissions near ports. Similar to the SV-OOA, the K and EC subgroups in the LV-OOA experienced a dramatic decline, with variance ratios of 112 and 58, respectively. To further illustrate the influence of land sources on the marine atmosphere during the LDP, we investigated the increasing process of SV-OOA and LV-OOA in Case 3. The average increase rates of the SV-OOA and LV-OOA were 0.58 and $0.33 \mu\text{g m}^{-3} \text{h}^{-1}$, respectively. Consistent with Case 1, SV-OOA exhibited a more obvious change during the LDP, and the EC and K subgroups were the most important species leading to SV-OOA and LV-OOA variation, respectively.

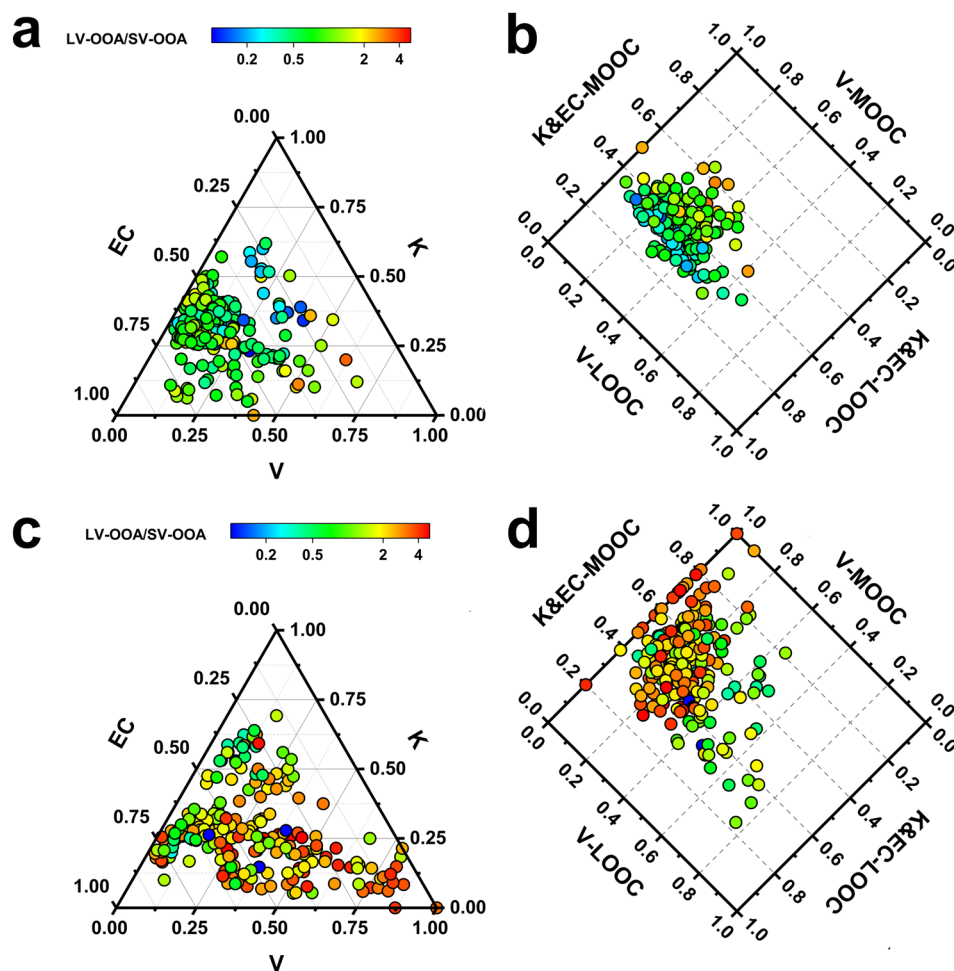


Fig. 4 The mixing state of OOA during two periods. Ternary plots for the EC, K, and V particles during **a** the LDP and **c** MDP. The EC, K, and V particles are normalized such that these three components comprise a total of 100%; the fractions of the LOOC and MOOC particles in the EC, K, and V particles during **b** the LDP and **d** MDP.

A clear difference in the growth processes during the MDP was observed in Case 2. Generally, a significant impact of ship emissions on the marine atmosphere was observed in Case 2. The average increase rates of the SV-OOA and LV-OOA particles were 0.24 and 0.20, respectively. The slightly lower increase rate of the LV-OOA was likely due to the smaller particle size of the V subgroup, which accounted for a large proportion of the LV-OOA. The V subgroup, an indicator of ship emissions, attained a variance rate of 272 in the LV-OOA, which was two times higher than that of the other subgroups, revealing the important contributions of ship emissions near ports.

DISCUSSION

The mass concentration of organics varied dramatically during the campaign, with the average concentration ranging from 1.46 to 5.04 $\mu\text{g m}^{-3}$. Accounting for 27–36% of all particles on average, organics comprised a major fraction of NR-PM₁ at all stages. Different LV-OOA/SV-OOA ratios were observed between the two periods, with a lower ratio during the LDP and a higher ratio during the MDP, suggesting a higher oxidation degree of OOA at stages with fewer land source influences. Besides, significant variance in the particle compositions of OOC particles was observed during these two periods. The EC and K subgroups yielded major contributions to LOOC and MOOC particles, respectively, during the LDP, which indicated that continental sources imposed a great effect on the marine aerosol environment

during these periods. With decreasing contribution of the K subgroup, the V subgroup played an increasingly important role in the MOOC particles during the MDP, suggesting that port and ship emissions also significantly influenced the offshore air environment in the ECS.

The different chemical compositions during the LDP and MDP were demonstrated as an important factor in the variance in the organic oxidation degree between these two periods. An increasing fraction of the V subgroup resulted in a higher oxidation degree during the MDP. Additionally, higher MOOC/LOOC ratios were observed in all subgroups during the MDP over the LDP, which further led to a higher oxidation degree during the MDP. Analysis of the ALWC and O₃ effects on OOA formation and MOOC/LOOC ratio in every subgroup suggested that photochemical oxidation was the dominant factor of the elevated oxidation degree during the MDP. These results suggest that both pollutant sources and oxidation processes are critical for organic aerosol characteristics and the oxidation degree in the offshore area of the ECS and anthropogenic activities should be considered in the occurrence, sources, and formation of OOA in the ECS.

METHODS

Sampling site and instrumentation

In situ measurements were conducted from 3 to 27 June 2017 in the offshore area of the ECS. The cruise campaign mainly surrounded the Zhoushan archipelago. The cruise track is depicted in Supplementary

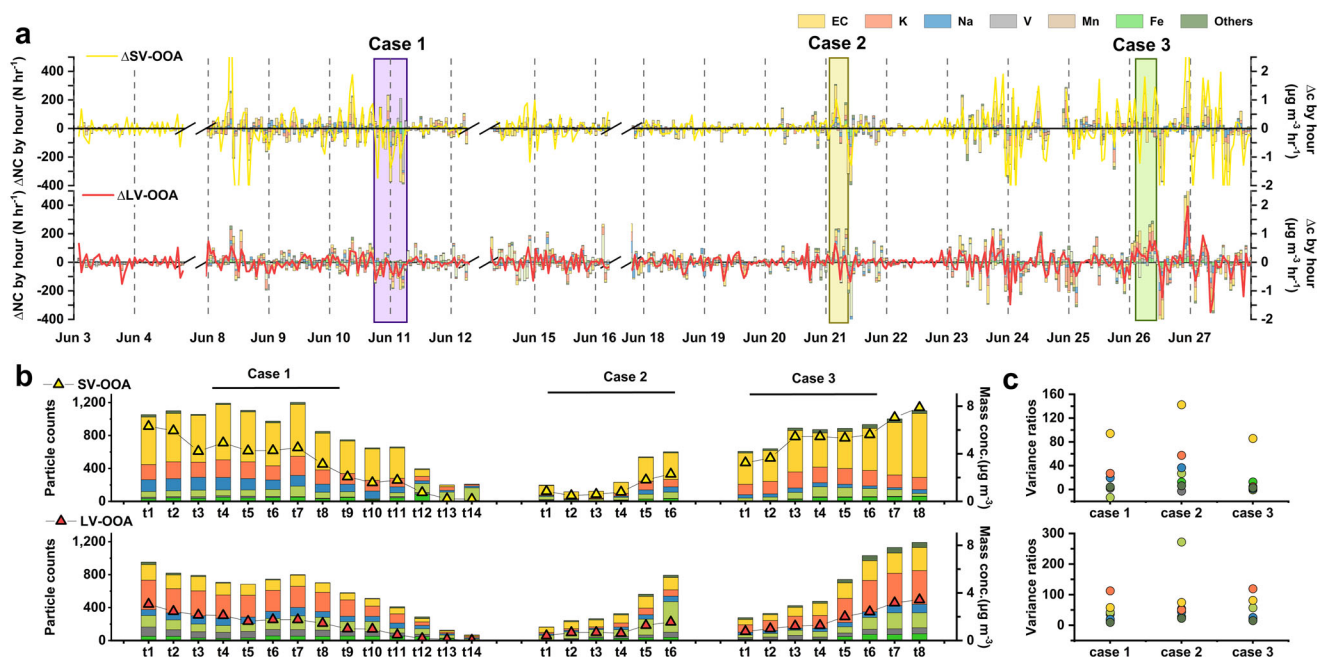


Fig. 5 Evolution patterns of OOA oxidation degree. **a** Variation rates of the OOA mass concentration with the ACSM instrument and OOC particle number concentration (NC) via SPAMS; **b** OOA mass concentration and OOC particle counts in the three typical cases; **c** the variation ratios of each subgroup in the three typical cases.

Fig. 2, and further details of the sampling site can be found elsewhere⁷⁷. All observational instruments were placed within a mobile platform located in the middle of a sampan. Trace constituents and meteorological parameters were continuously measured during the cruise campaign.

All observational instruments were placed within a mobile platform located in the middle of a sampan. Trace constituents and meteorological parameters were continuously measured during the cruise campaign¹⁹. Basically, this instrument is composed of an aerodynamic lens that focuses a particle beam (with a vacuum aerodynamic diameter below 1 μm) and directs it through three vacuum chambers, the last one being a detection chamber in which particles are vaporized upon impact on a surface heated to 600 $^{\circ}\text{C}$. The generated positive ions were finally analyzed with a commercial quadrupole mass spectrometer.

The SPAMS instrument (Guangzhou Hexin Analytical Company) employed in this work was designed according to the ATOFMS method and has been introduced in detail in the previous publications⁷⁸. Briefly, ambient particles were sampled through an 80 μm critical orifice into a vacuum-controlled aerodynamic lens at a flow rate of 75 mL min^{-1} . The size of individual particles was measured by two laser beams (532 nm) and subsequently desorbed or ionized by a pulsed laser (266 nm). After ionization, the positive and negative ions were detected with a Z-shaped bipolar time-of-flight mass spectrometer.

Data analysis

The final mass concentrations and mass spectra were processed in ACSM standard data software, which is a widely applied procedure described in ref. ¹⁹. A particle collection efficiency (CE) of 0.5 was attained throughout the entire campaign. The mass concentration and chemical composition of NR-PM₁ species were obtained based on the default relative ionization efficiency (RIE), at 1.4, 1.2, 1.1, and 1.3 for Org, SO₄, NO₃, NH₄, and Cl, respectively, and an RIE value of 5.72 for ammonium based on on-site calibrations. Source apportionment of the organics was conducted via PMF, and the results were evaluated with the Igor Pro-based PMF Evaluation Tool. Three factors, HOA, SV-OOA, and LV-OOA were identified.

The size distributions and chemical compositions of the particles detected by SPAMS were analyzed using the YAADA software based on MATLAB software toolkit. A total of 546,874 particles with both positive and negative ion mass spectra were collected during the campaign. In previous SPAMS studies, 27[C₂H₃]⁺, 37[C₃H]⁺, and 43[C₂H₃O]⁺ have been identified as markers for organic compounds both in field and laboratory measurements^{30,79,80}. Thus, in this study, oxidized organic carbon (OOC) particles were identified by organic markers with relative peak areas larger

than 5%. OOC particles with higher organic signals (greater than 10%) were identified as more oxidized organic carbon (MOOC) particles, and the remaining particles were identified as less oxidized organic carbon (LOOC) particles. According to this classification criterion, a total of 309,914 OOC particles were identified, of which 156,008 and 153,906 particles were identified as LOOC and MOOC particles, respectively. Furthermore, all the OOC particles were classified into seven subgroups with the ART-2a method to investigate their sources and formation process. The seven subgroups of OOC particles included (1) the elemental carbon (EC) subgroup, (2) K subgroup, (3) Na subgroup, (4) V subgroup, (5) Mn subgroup, (6) Fe subgroup, and (7) other subgroup.

Air mass backward trajectories

Air masses related to local or regional meteorological conditions could be responsible for the atmospheric transport of aerosol particles along with the vertical and horizontal directions. Twenty-four hours air mass backward trajectories for each day were simulated with the Hybrid Single-Particle Lagrangian Integrated Trajectory (HYSPPLIT, http://www.arl.noaa.gov/HYSPPLIT_info.php) model of the National Oceanic and Atmospheric Administration (NOAA) Air Resources Laboratory (ARL) and were calculated at 0:00, 6:00, 12:00, and 18:00 (local time) at a height of 500 m (Supplementary Fig. 1).

NR-PM₁ mass concentration variation processes

In this study, we calculated the variation rate for two OOA mass concentrations and the particle numbers of seven OOC subgroups to illustrate organic compound variation processes. The variation rates of the OOA and OOC subgroups were defined with Eq. (1) and Eq. (2), respectively:

$$\text{Variation rate } (\mu\text{g} \cdot \text{m}^{-3} \cdot \text{h}^{-1}) = \frac{([\text{mass concentration}]_{n+t} - [\text{mass concentration}]_t)}{n \text{ (hour)}} \quad (1)$$

$$\text{Variation rate } (\text{N} \cdot \text{h}^{-1}) = \frac{([\text{particle number}]_{n+t} - [\text{particle number}]_t)}{n \text{ (hour)}} \quad (2)$$

the variation ratio of the seven OOC subgroups was calculated to evaluate the contribution of each subgroup to OOA variation, and the variation ratio was determined with Eq. (3):

$$\text{Variation ratio } (\text{N}/\mu\text{g} \cdot \text{m}^{-3}) = \frac{([\text{particle number}]_{\text{end}} - [\text{particle number}]_{\text{start}})}{([\text{mass concentration}]_{\text{end}} - [\text{mass concentration}]_{\text{start}})} \quad (3)$$

DATA AVAILABILITY

Raw data used in this study are archived at the Department of Environmental Science & Engineering, Fudan University, and are available on request by contacting the corresponding author (jmchen@fudan.edu.cn).

Received: 24 January 2022; Accepted: 13 May 2022;

Published online: 09 June 2022

REFERENCES

- Hallquist, M. et al. The formation, properties and impact of secondary organic aerosol: current and emerging issues. *Atmos. Chem. Phys.* **9**, 5155–5236 (2009).
- Jimenez, J. L. et al. Evolution of organic aerosols in the atmosphere. *Science* **326**, 1525–1529 (2009).
- Kanakidou, M. et al. Organic aerosol and global climate modelling: a review. *Atmos. Chem. Phys.* **5**, 1053–1123 (2005).
- Zhang, Q. et al. Ubiquity and dominance of oxygenated species in organic aerosols in anthropogenically-influenced Northern Hemisphere midlatitudes. *Geophys. Res. Lett.* **34**, L13801 (2007).
- Ervens, B., Turpin, B. J. & Weber, R. J. Secondary organic aerosol formation in cloud droplets and aqueous particles (aqSOA): a review of laboratory, field and model studies. *Atmos. Chem. Phys.* **11**, 11069–11102 (2011).
- Tröstl, J. et al. The role of low-volatility organic compounds in initial particle growth in the atmosphere. *Nature* **533**, 527–531 (2016).
- Lelieveld, J., Evans, J. S., Fnais, M., Giannadaki, D. & Pozzer, A. The contribution of outdoor air pollution sources to premature mortality on a global scale. *Nature* **525**, 367–371 (2015).
- Clancy, L., Goodman, P., Sinclair, H. & Dockery, D. W. Effect of air-pollution control on death rates in Dublin, Ireland: an intervention study. *Lancet* **360**, 1210–1214 (2002).
- Zanobetti, A., Austin, E., Coull, B. A., Schwartz, J. & Koutrakis, P. Health effects of multi-pollutant profiles. *Environ. Int.* **71**, 13–19 (2014).
- Porter, W. C., Jimenez, J. L. & Barsanti, K. C. Quantifying atmospheric parameter ranges for ambient secondary organic aerosol formation. *ACS Earth Space Chem.* **5**, 2380–2397 (2021).
- Aiken, A. C. et al. Mexico City aerosol analysis during MILAGRO using high resolution aerosol mass spectrometry at the urban supersite (T0)—Part 1: Fine particle composition and organic source apportionment. *Atmos. Chem. Phys.* **9**, 6633–6653 (2009).
- Sun, Y. L. et al. Aerosol composition, sources and processes during wintertime in Beijing, China. *Atmos. Chem. Phys.* **13**, 4577–4592 (2013).
- Zhang, Q. et al. Understanding atmospheric organic aerosols via factor analysis of aerosol mass spectrometry: a review. *Anal. Bioanal. Chem.* **401**, 3045–3067 (2011).
- Sun, Y. et al. Investigation of the sources and evolution processes of severe haze pollution in Beijing in January 2013. *J. Geophys. Res. Atmos.* **119**, 4380–4398 (2014).
- Crippa, M. et al. Wintertime aerosol chemical composition and source apportionment of the organic fraction in the metropolitan area of Paris. *Atmos. Chem. Phys.* **13**, 961–981 (2013).
- Lee, B. P., Li, Y. J., Yu, J. Z., Louie, P. K. K. & Chan, C. K. Characteristics of submicron particulate matter at the urban roadside in downtown Hong Kong—Overview of 4 months of continuous high-resolution aerosol mass spectrometer measurements. *J. Geophys. Res. Atmos.* **120**, 7040–7058 (2015).
- Hu, W. et al. Evaluation of the new capture vaporizer for aerosol mass spectrometers (AMS) through field studies of inorganic species. *Aerosol Sci. Technol.* **51**, 735–754 (2017).
- Allan, J. D. et al. Contributions from transport, solid fuel burning and cooking to primary organic aerosols in two UK cities. *Atmos. Chem. Phys.* **10**, 647–668 (2010).
- Ng, N. L. et al. An aerosol Chemical speciation monitor (ACSM) for routine monitoring of the composition and mass concentrations of ambient aerosol. *Aerosol Sci. Technol.* **45**, 780–794 (2011).
- Sun, Y. et al. Primary and secondary aerosols in Beijing in winter: sources, variations and processes. *Atmos. Chem. Phys.* **16**, 8309–8329 (2016).
- Chen, Y. et al. Chemical characterization of secondary organic aerosol at a rural site in the southeastern US: insights from simultaneous high-resolution time-of-flight aerosol mass spectrometer (HR-ToF-AMS) and FIGAERO chemical ionization mass spectrometer (CIMS) measurements. *Atmos. Chem. Phys.* **20**, 8421–8440 (2020).
- Li, H. et al. Characteristics and sources of water-soluble organic aerosol in a heavily polluted environment in Northern China. *Sci. Total Environ.* **758**, 143970 (2021).
- Cash, J. M. et al. Seasonal analysis of submicron aerosol in Old Delhi using high-resolution aerosol mass spectrometry: chemical characterisation, source apportionment and new marker identification. *Atmos. Chem. Phys.* **21**, 10133–10158 (2021).
- Zhang, X., Xu, J., Kang, S. & Zhang, Q. Chemical characterization and sources of submicron aerosols in the northeastern Qinghai-Tibet Plateau: insights from high-resolution mass spectrometry. *Atmos. Chem. Phys.* **19**, 1–19 (2019).
- Li, J. et al. Highly time-resolved chemical characterization and implications of regional transport for submicron aerosols in the North China Plain. *Sci. Total Environ.* **705**, 135803 (2020).
- Zhu, Q. et al. Atmospheric aerosol compositions and sources at two national background sites in northern and southern China. *Atmos. Chem. Phys.* **16**, 10283–10297 (2016).
- Pratt, K. A. & Prather, K. A. Mass spectrometry of atmospheric aerosols—recent developments and applications. Part II: On-line mass spectrometry techniques. *Mass Spectrom. Rev.* **31**, 17–48 (2012).
- Murphy, D. M. et al. Single-particle mass spectrometry of tropospheric aerosol particles. *J. Geophys. Res. Atmos.* **111**, D23S32 (2006).
- Pratt, K. A. et al. Flight-based chemical characterization of biomass burning aerosols within two prescribed burn smoke plumes. *Atmos. Chem. Phys.* **11**, 12549–12565 (2011).
- Zhang, G. et al. Mixing state of individual submicron carbon-containing particles during spring and fall seasons in urban Guangzhou, China: a case study. *Atmos. Chem. Phys.* **13**, 4723–4735 (2013).
- Zhang, G. et al. Source and mixing state of iron-containing particles in Shanghai by individual particle analysis. *Chemosphere* **95**, 9–16 (2014).
- Silva, P. J., Liu, D.-Y., Noble, C. A. & Prather, K. A. Size and chemical characterization of individual particles resulting from biomass burning of local southern California species. *Environ. Sci. Technol.* **33**, 3068–3076 (1999).
- Cho, H.-j. et al. Application of single-particle mass spectrometer to obtain chemical signatures of various combustion aerosols. *Int. J. Environ. Res. Public Health* **18**, 11580 (2021).
- Healy, R. et al. Characterisation of single particles from in-port ship emissions. *Atmos. Environ.* **43**, 6408–6414 (2009).
- Whiteaker, J. R., Suess, D. T. & Prather, K. A. Effects of meteorological conditions on aerosol composition and mixing state in Bakersfield, CA. *Environ. Sci. Technol.* **36**, 2345–2353 (2002).
- Bi, X. et al. Mixing state of biomass burning particles by single particle aerosol mass spectrometer in the urban area of PRD, China. *Atmos. Environ.* **45**, 3447–3453 (2011).
- Fu, H. et al. Sources and characteristics of fine particles over the Yellow Sea and Bohai Sea using online single particle aerosol mass spectrometer. *J. Environ. Sci. (China)* **29**, 62–70 (2015).
- Middlebrook, A. M. et al. A comparison of particle mass spectrometers during the 1999 Atlanta Supersite Project. *J. Geophys. Res. Atmos.* **108**, 8424 (2003).
- Salcedo, D. et al. Determination of particulate lead using aerosol mass spectrometry: MILAGRO/MCMA-2006 observations. *Atmos. Chem. Phys.* **10**, 5371–5389 (2010).
- Xing, J.-H. et al. Characterization of aerosol particles in the Tokyo Metropolitan area using two different particle mass spectrometers. *Aerosol Sci. Technol.* **45**, 315–326 (2011).
- Drewnick, F., Dall’osto, M. & Harrison, R. Characterization of aerosol particles from grass mowing by joint deployment of ToF-AMS and ATOFMS instruments. *Atmos. Environ.* **42**, 3006–3017 (2008).
- Cubison, M. J. et al. The influence of chemical composition and mixing state of Los Angeles urban aerosol on CCN number and cloud properties. *Atmos. Chem. Phys.* **8**, 5649–5667 (2008).
- Charlson, R. J., Lovelock, J. E., Andreae, M. O. & Warren, S. G. Oceanic phytoplankton, atmospheric sulphur, cloud albedo and climate. *Nature* **326**, 655–661 (1987).
- O’Dowd, C. D. et al. Biogenically driven organic contribution to marine aerosol. *Nature* **431**, 676–680 (2004).
- Zheng, G. et al. New particle formation in the remote marine boundary layer. *Nat. Commun.* **12**, 527 (2021).
- Tsai, H.-H. Physicochemical Properties of PM_{2.5} and PM_{2.5–10} at inland and offshore sites over southeastern coastal region of Taiwan Strait. *Aerosol Air Qual. Res.* **11**, 664–678 (2011).
- Pandolfi, M. et al. Source apportionment of PM₍₁₀₎ and PM_(2.5) at multiple sites in the strait of Gibraltar by PMF: impact of shipping emissions. *Environ. Sci. Pollut. Res.* **18**, 260–269 (2011).
- Pey, J., Pérez, N., Cortés, J., Alastuey, A. & Querol, X. Chemical fingerprint and impact of shipping emissions over a western Mediterranean metropolis: primary and aged contributions. *Sci. Total Environ.* **463–464**, 497–507 (2013).
- Johnson, G. et al. Relating urban airborne particle concentrations to shipping using carbon based elemental emission ratios. *Atmos. Environ.* **95**, 525–536 (2014).
- van Pinxteren, M. et al. Chemical characterization of sub-micrometer aerosol particles in the tropical Atlantic Ocean: marine and biomass burning influences. *J. Atmos. Chem.* **72**, 105–125 (2015).

51. Zhao, M. et al. Characteristics and ship traffic source identification of air pollutants in China's largest port. *Atmos. Environ.* **64**, 277–286 (2013).
52. Xu, L. et al. Source identification of PM_{2.5} at a port and an adjacent urban site in a coastal city of China: impact of ship emissions and port activities. *Sci. Total Environ.* **634**, 1205–1213 (2018).
53. Viana, M. et al. Chemical tracers of particulate emissions from commercial shipping. *Environ. Sci. Technol.* **43**, 7472–7477 (2009).
54. Cesari, D. et al. Source apportionment of PM_{2.5} in the harbor-industrial area of Brindisi (Italy): identification and estimation of the contribution of in-port ship emissions. *Sci. Total Environ.* **497–498C**, 392–400 (2014).
55. Koçak, M. et al. Particulate matter (PM₁₀) in Istanbul: Origin, source areas and potential impact on surrounding regions. *Atmos. Environ.* **45**, 6891–6900 (2012).
56. Pérez, N. et al. Impact of harbour emissions on ambient PM₁₀ and PM_{2.5} in Barcelona (Spain): evidences of secondary aerosol formation within the urban area. *Sci. Total Environ.* **571**, 237–250 (2016).
57. Diapouli, E. et al. Evolution of air pollution source contributions over one decade, derived by PM₁₀ and PM_{2.5} source apportionment in two metropolitan urban areas in Greece. *Atmos. Environ.* **164**, 416–430 (2017).
58. Contini, D. et al. The direct influence of ship traffic on atmospheric PM_{2.5}, PM₁₀ and PAH in Venice. *J. Environ. Manag.* **92**, 2119–2129 (2011).
59. Bove, M. C. et al. An integrated PM_{2.5} source apportionment study: positive Matrix Factorisation vs. the chemical transport model CAMx. *Atmos. Environ.* **94**, 274–286 (2014).
60. O'Dowd, C. D. & de Leeuw, G. Marine aerosol production: a review of the current knowledge. *Philos. Trans. R. Soc., A* **365**, 1753–1774 (2007).
61. Agrawal, H., Malloy, Q. G. J., Welch, W. A., Miller, J. W. & Cocker, D. R. In-use gaseous and particulate matter emissions from a modern ocean going container vessel. *Atmos. Environ.* **42**, 5504–5510 (2008).
62. Ault, A. P. et al. Characterization of the single particle mixing state of individual ship plume events measured at the port of Los Angeles. *Environ. Sci. Technol.* **44**, 1954–1961 (2010).
63. Corbett, J. J. et al. Mortality from ship emissions: a global assessment. *Environ. Sci. Technol.* **41**, 8512–8518 (2007).
64. Du, W. et al. Chemical characterization of submicron aerosol and particle growth events at a national background site (3295 m a.s.l.) on the Tibetan Plateau. *Atmos. Chem. Phys.* **15**, 10811–10824 (2015).
65. Narukawa, M. et al. Single particle analysis of secondary organic aerosols formed from 1,4-Cyclohexadiene ozonolysis using a laser-ionization single-particle aerosol mass spectrometer. *Bull. Chem. Soc. Jpn.* **81**, 120–126 (2008).
66. Murphy, S. M. et al. Comprehensive simultaneous shipboard and airborne characterization of exhaust from a modern container ship at sea. *Environ. Sci. Technol.* **43**, 4626–4640 (2009).
67. Wu, D., Zhang, F., Lou, W., Li, D. & Chen, J. Chemical characterization and toxicity assessment of fine particulate matters emitted from the combustion of petrol and diesel fuels. *Sci. Total Environ.* **605–606**, 172–179 (2017).
68. Echalar, F., Gaudichet, A., Cachier, H. & Artaxo, P. Aerosol emissions by tropical forest and savanna biomass burning: Characteristic trace elements and fluxes. *Geophys. Res. Lett.* **22**, 3039–3042 (1995).
69. Wang, W. et al. Sulfate formation is dominated by manganese-catalyzed oxidation of SO₂ on aerosol surfaces during haze events. *Nat. Commun.* **12**, 1993 (2021).
70. Gong, H. et al. The enhanced mixing states of oxalate with metals in single particles in Guangzhou, China. *Sci. Total Environ.* **783**, 146962 (2021).
71. Canagaratna, M. R. et al. Elemental ratio measurements of organic compounds using aerosol mass spectrometry: characterization, improved calibration, and implications. *Atmos. Chem. Phys.* **15**, 253–272 (2015).
72. Xu, J. et al. Chemical composition, sources, and processes of urban aerosols during summertime in northwest China: insights from high-resolution aerosol mass spectrometry. *Atmos. Chem. Phys.* **14**, 12593–12611 (2014).
73. Chakraborty, A. & Riffault, V. Real-time assessment of wintertime organic aerosol characteristics and sources at a suburban site in northern France. *Atmos. Environ.* **203**, 48–61 (2019).
74. Chen, T. et al. Chemical characterization of submicron aerosol in summertime Beijing: a case study in southern suburbs in 2018. *Chemosphere* **247**, 125918 (2020).
75. Ng, N. L. et al. Changes in organic aerosol composition with aging inferred from aerosol mass spectra. *Atmos. Chem. Phys.* **11**, 6465–6474 (2011).
76. Zhan, B. et al. The roles of aqueous-phase chemistry and photochemical oxidation in oxygenated organic aerosols formation. *Atmos. Environ.* **266**, 118738 (2021).
77. Liu, Z. et al. Size-resolved mixing states and sources of amine-containing particles in the East China Sea. *J. Geophys. Res. Atmos.* **125**, e2020JD033162 (2020).
78. Lei, L. et al. Real time bipolar time-of-flight mass spectrometer for analyzing single aerosol particles. *Int. J. Mass Spectrom.* **303**, 118–124 (2011).
79. Cheng, C. et al. Single particle diversity and mixing state of carbonaceous aerosols in Guangzhou, China. *Sci. Total Environ.* **754**, 142182 (2021).
80. Huang, M. et al. Laser desorption/ionization mass spectrometric study of secondary organic aerosol formed from the photooxidation of aromatics. *J. Atmos. Chem.* **58**, 237–252 (2007).

ACKNOWLEDGEMENTS

This work was funded by the National Natural Science Foundation of China (Nos. 91743202, 91843301, 92043301, and 21527814), Science & Technology Commission of Shanghai Municipality (No. 21DZ1202300), and Shanghai International Science and Technology Partnership Project (No. 21230780200).

AUTHOR CONTRIBUTIONS

Z.L. analyzed the data and wrote the manuscript; H.C. and J.C. designed the study, reviewed, and edited the manuscript; L.L., G.X., and H.O. helped the data analysis; X.T., R.J., B.L., and R.Z. edited the manuscript. All authors contributed to the discussion and revision.

COMPETING INTERESTS

The authors declare no competing interests.

ADDITIONAL INFORMATION

Supplementary information The online version contains supplementary material available at <https://doi.org/10.1038/s41612-022-00267-1>.

Correspondence and requests for materials should be addressed to Hui Chen or Jianmin Chen.

Reprints and permission information is available at <http://www.nature.com/reprints>

Publisher's note Springer Nature remains neutral with regard to jurisdictional claims in published maps and institutional affiliations.



Open Access This article is licensed under a Creative Commons Attribution 4.0 International License, which permits use, sharing, adaptation, distribution and reproduction in any medium or format, as long as you give appropriate credit to the original author(s) and the source, provide a link to the Creative Commons license, and indicate if changes were made. The images or other third party material in this article are included in the article's Creative Commons license, unless indicated otherwise in a credit line to the material. If material is not included in the article's Creative Commons license and your intended use is not permitted by statutory regulation or exceeds the permitted use, you will need to obtain permission directly from the copyright holder. To view a copy of this license, visit <http://creativecommons.org/licenses/by/4.0/>.

© The Author(s) 2022